Crystal growth in nanoporous framework materials†

Michael W. Anderson,* Jonathan R. Agger, L. Itzel Meza, Chin B. Chong and Colin S. Cundy

Received 5th December 2006, Accepted 30th January 2007
First published as an Advance Article on the web 10th April 2007
DOI: 10.1039/b617782b

Future applications of nanoporous materials will be in opto-electronic devices, magnetic and chemical sensors, shape-selective and bio-catalysis, structural materials and nuclear waste management. Crucially, in all such applications, an understanding of crystal growth to the same depth as has been achieved in semiconductor technology is needed. Therefore, defects, intergrowths, dopants and isomorphous substitution must be controlled, and crystal habit and size (*e.g.* single crystal films) must be fabricated with precision. These goals elude the community because of lack of understanding of crystal growth processes. Modern microscopy techniques including AFM, ultra-high resolution SEM and HREM coupled with theoretical calculations are beginning to reveal the details of these growth processes yielding the important thermodynamic data crucial to effect synthetic control such as: controlling defects; controlling intergrowths; introducing chirality; modifying surface access; altering diffusion pathways; controlling crystal habit; synthesising templated materials cheaply in order to render them economically viable; controlling crystal size for instance as single crystal films. In this paper we will discuss recent results including: the details of surface alteration processes in nanoporous materials, measured *in situ*, under different chemical environments and the ability to switch processes on and off by the control of growth conditions. Further we illustrate an approach to theoretically model the crystal growth in such complex systems which ultimately delivers activation energies for fundamental growth processes.

Introduction

Crystal growth in nanoporous framework materials is a subject that has received considerable attention over many decades.[1,2] This interest has been fueled by the enormous industrial significance of this class of material in the areas of petrochemicals, ion-exchange and gas separation. Indeed much of this work has been performed within an industrial setting with the goal normally to synthesise new crystalline phases with desired pore architecture and functionality. Crystal size and morphology are important for many of these applications.[3] For instance, for

Centre for Nanoporous Materials, School of Chemistry, The University of Manchester, Oxford Road, Manchester, UK M13 9PL. E-mail: m.anderson@manchester.ac.uk; Fax: +44 161 306 4551; Tel: +44 161 306 4517

† We would like to acknowledge the assistance of R. J. Plaisted for help with the continuous flow experiments. Also to EPSRC and ExxonMobil for funding.

application in catalysis it is often important to limit crystal size in order to reduce diffusion path-lengths from the crystal periphery to the internal void space. For similar reasons, when the pore structure is anisotropic, such as in a material with unidimensional porosity, it is important to reduce the crystal size along the direction of these pores. As many zeolites with unidimensional pores have a natural tendency to grow with a long crystal dimension parallel to the pores, this requires a modification of the crystal morphology or aspect ratio.[4] As with most synthetic work these desired effects can often be achieved using an informed trial-and-error approach coupled with high-throughput synthetic methods.[5] However, the phase space is enormous (incorporating both inorganic and organic components) and even high-throughput methods are hampered by the mechanical complexity of developing a robotic approach for every synthetic and characterisation step associated with this kind of work. Nevertheless, it could be argued that the subject had reached a reasonable degree of maturity by the early 1990s despite quite a range of new zeolitic and related phases being discovered since this time.[6]

New impetus to the study of crystal growth in many fields, including nanoporous framework materials, was ignited with the advent of scanning probe microscopy methods.[7] This opened up a considerable new level of detail, with possibilities for monitoring growth processes at the molecular scale, *in situ*, thereby extracting detailed growth mechanisms and related thermodynamic constants. In practice realisation of this is far from straightforward: first, because the experimental procedures are delicate; second, because the theoretical models to simulate experimental results are not in place and must be developed from scratch.

In this paper we discuss results from atomic force microscopy, AFM, applied to zeolite A and the siliceous analogue of zeolite ZSM-5 known as silicalite. The experimental methodology involves a combination of *ex situ* and *in situ* AFM. The former approach is the most flexible allowing crystals to be grown under conditions which are not suitable for the microscope but optimised to answer specific questions. Following crystallisation under controlled conditions the crystals are transferred to the atomic force microscope. The *in situ* measurements by contrast need to be designed to be compatible with the atomic force microscope. For zeolite preparations desirable conditions for growth would often necessitate growth from a gel phase. This is incompatible with the microscope as the laser cannot penetrate the cloudy suspension. For this reason we restrict ourselves in this paper to discussions of dissolution experiments under clear basic conditions. A further important requirement for the study of crystal growth or dissolution is that the kinetics must be slow enough to be captured at a frame rate of *ca.* 1–2 min. Such a slow rate means that supersaturation must be adjusted close to equilibrium conditions and consequently the thermodynamics will be that associated with near equilibrium.

In order to interpret the AFM results it is necessary to simulate surface topography.[8] In this paper we demonstrate a method which is able to simulate crystal growth in a nanoporous framework material from which fundamental growth rates can be extracted. In order to maximise the experimental input to the simulations we adopt an approach which endeavours to simulate both crystal habit and surface topography using one set of growth parameters. At present the method is hard-wired to simulate growth in cubic systems but the same general approach could be used to simulate crystal growth in any crystal system.

Setting the scene

The fundamental importance of the nanoporous class of materials which include zeolites is the nature and accessibility of the internal pore structure which imparts very high surface area and also high selectivity for molecular recognition. For zeolites the accessibility and integrity of this pore structure is governed by the precise nature of the crystal. Fig. 1 shows three examples of crystals of zeotype materials. The upper image shows small 5 μm crystals of the siliceous microporous material

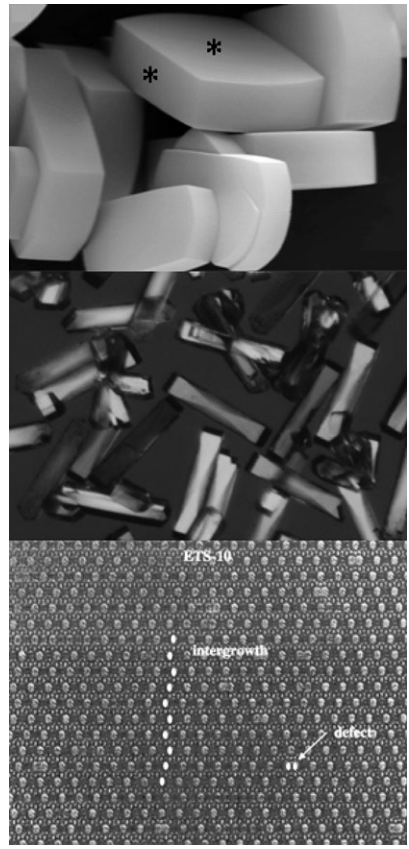

Fig. 1 Upper, SEM shows 5 μm near perfect crystals of silicalite, tunnels exit on facets marked with *. Middle, large 280 μm long silicalite crystals exhibiting faulted structure. Lower, HREM of microporous titanosilicate ETS-10 showing details of defects and intergrowth, pore size *ca.* 7 Å.

silicalite. The crystals have been grown at a comparatively low temperature of 130 °C and the morphology is indicative of crystals with low defect concentration and no intergrowths. In other words the crystal form is as near perfect as might be expected. The pore structure of silicalite is two dimensional with tunnels exiting the crystal surface on the two flat facets marked with an asterisk. The aspect ratio of the crystal defines the overall tunnel length which is consequently different in different directions. The middle image shows the same crystal structure, silicalite, grown at a much higher temperature, 180 °C, which produces much larger crystals, *ca.* 180 μm in length and modified aspect ratio and overall habit. Most strikingly in the optical micrograph of these crystals is the birefringent *hour-glass* effect which is due to internal faulting. This faulting will directly affect the diffusion of guest gas molecules through the pore network. Finally, the lower high-resolution electron micrograph of the microporous titanosilicate ETS-10 shows that the *normal* structure contains both defects and intergrowths. The defects are very well defined structural imperfections, in this case double pores, and the intergrowth is a random connection of the pore structure which is built up of layers from the bottom of the image to the top. The defects will affect porosity and thereby selectivity of the crystal but also the thermal and hydrothermal stability of the material. The intergrowth changes the entire structure, one possible ordered intergrowth of ETS-10 exhibits a spiral pore in one direction.[9] All the features discussed in these examples should be controllable if it is

possible to understand and control crystal growth. Crystal aspect ratio becomes particularly important for structures with unidimensional pores (such as zeolite L[4]) where typically the crystals form needles with the pores along the long needle direction. For catalytic purposes this is undesirable as short diffusion path-lengths are preferred in order to increase accessibility to the internal pore space. Another very important factor which must be considered in the synthesis of microporous structures is the cost of any organic template (or structure-directing agent, SDA). Such molecules are crucial for the synthesis of the vast majority of zeotype materials and preclude the preparation for commercial purposes on the basis of cost. Reducing the amounts, or elimination of the SDA, is a highly desirable goal to attain. Another aspect which is of interest is the size of the crystal—most microporous materials grow as micron-sized crystals. This is ideal for catalysis where the smaller the crystal usually the more active the catalyst. However, for opto-electronic device technology large crystals are preferred. Similarly single crystal films would be of great interest for separation applications. All these desires elude the community at present because our understanding of the fundamental growth processes is insufficient. Consequently, the goal of our work on crystal growth in nanoporous materials is to be able to ultimately exert control over the following important parameters:

- Defects
- Intergrowths
- Introduction of chirality
- Surface access
- Diffusion pathways
- Crystal habit (*e.g.* short *c*-axis)
- Template (especially for cheaper synthesis)
- Crystallite size (*e.g.* single crystal films)

The strategy that we adopt along with collaborators in Stockholm, Lund, Versailles, Royal Institution, UCL and Bath[10] to tackle these problems is interdisciplinary but relies heavily on microscopy techniques in particular: *in situ* and *ex situ* atomic force microscopy; very high-resolution scanning electron microscopy; high-resolution electron microscopy. This is coupled with theoretical calculations of surface energies and growth pathways and simulations of surface topologies and crystal habit. These theoretical methods lead to rate constants for fundamental growth processes. Finally we are utilising NMR and mass spectrometry methods to look at solution speciation within the mother liquor from which the crystals grow.[11] This contribution details results from recent AFM measurements coupled with simulation of the experimental data.

Experimental

The zeolite A crystals were synthesized from a gel with molar composition SiO_2 : 2.23 Na_2O : 5.18 TEA : 0.89 Al_2O_3 : 246 H_2O. Two solutions were prepared as follows: solution 1, 0.85 g aluminum wire (BDH) was dissolved in an alkaline solution of 3.14 g NaOH (BDH) dissolved in 39.39 mL deionised water, the final mixture was filtered to remove impurities; solution 2 was prepared by adding 3.65 g tetraethyl orthosilicate (TEOS from Aldrich) to a solution of 13.57 g triethanolamine (TEA from Acros organics) and 39.39 g water. Both solutions were mixed with vigorous stirring and then aged for 30 min in polypropylene bottles.

Atomic force micrographs were recorded on a Digital Instruments MultiMode™ SPM with Nanoscope III controller using AFM Contact Mode with 0.58 N m^{-1} force constant silicon nitride tips at scan rates of 3 Hz. A syringe pump (Razel™ model A-99 from SEMAT) was used for the experiments conducted under continuous flow. All experiments were carried out at room temperature, 25 °C. Errors in terrace heights were determined by measuring at least 50 separate heights.

1.6 μm long, un-twinned, lozenge-shaped silicalite seed crystals were synthesised as detailed elsewhere.[12] Seed crystals at a concentration of 9.5 g L^{-1} in their spent

mother liquor were placed in a specially modified 1 L autoclaved reactor stirred at 300 rpm. The slurry was heated to 130 °C over a period of 30 min and then left to equilibrate for 3 h, after which nutrient feed was switched on at an initial rate of 90 mL h^{-1}. The nutrient feed comprised silica sol, tetrapropylammonium bromide and sodium hydroxide with the following composition [Si] = 0.48 M, Si : OH = 8.72 and Si : TPA = 10.00. Samples were removed at regular intervals in order to maintain an effectively constant working volume in the reactor. In the absence of secondary nucleation, the assumption of effective stirring to create homogeneous crystal distribution enabled calculation and monitoring of the required nutrient feed to produce constant linear crystal growth rates of 0.4 μm h^{-1}. During the course of the reaction the nutrient feed was disconnected for periods of *ca.* 16 h allowing gel depletion akin to the latter stages of a normal batch synthesis. Quoted reaction times refer to the total period for which the nutrient feed was switched on.

The simulation of micrographs was performed using a computer model written in Fortran. Graphical output from the program is produced using Mathematica.

Zeolite A dissolution

Understanding precisely which structural units attach to the crystal surface from solution is a difficult problem to solve. Techniques, such as NMR and mass spectrometry[11,13] may be applied to monitor solution speciation, however, it is usually difficult to differentiate spectator species from active species in solution. One technique which has been successfully adopted to determine the species which attach to the solid for nanoporous aluminophosphates[14] is to look at the reverse dissolution reaction. Under favourable conditions the rate constants for competitive processes result in high concentrations of the active species being formed by the dissolution process whereas high concentrations of spectator species are formed during the growth process. With a similar purpose in mind we have monitored the dissolution of zeolite A using *in situ* AFM.

Fig. 2 shows a series of images showing the dissolution of the (100) facet of zeolite A under 0.5 M NaOH solution recorded every three minutes. The schematic on the right depicts the changes in the surface topology during this treatment. The 1.2 ± 0.1 nm high square terraces dissolve initially *via* terrace retreat. The terrace height corresponds to half a unit cell consisting of one sodalite cage and a double 4-ring (see Fig. 3). Interestingly the straight edges of the terraces dissolve more slowly than the holes in the terraces which open up preferentially. This is in accordance with our previous work on growth of zeolite A which showed that growth at kink sites is about 15 times faster than growth at edge sites.[8] The curved terrace edges present in the holes will show a high kink site density compared to the straight terrace edges and, consequently, it appears that dissolution is also favoured at kink sites over edge sites. The height of the receding terrace edge is only 0.9 ± 0.1 nm rather than the full 1.2 ± 0.1 nm. Indeed the remaining 0.3 ± 0.1 nm can be seen as an undisturbed terrace edge which is depicted as a dotted line in the schematic in Fig. 2. Consequently, there is a second structure 0.3 ± 0.1 nm in height which is more stable than the 0.9 ± 0.1 nm structure. The final dissolution of the top terrace occurs as the terrace breaks up into smaller squares which are rather uniform and *ca.* 90 × 90 × 9 nm in size. This phenomenon can be seen even more clearly in Fig. 4. After the 0.9 ± 0.1 nm high terrace is removed the dissolution repeats and another terrace is removed which is 0.9 ± 0.1 nm high. This means that dissolution of the intervening 0.3 ± 0.1 nm high terrace is not observed by AFM. The most likely explanation for this is that the 0.3 ± 0.1 nm high terrace dissolves orthogonal to the surface. This can be understood by careful consideration of the structure of zeolite A. Zeolite A is composed of sodalite cages (truncated octahedra) connected to each other by double 4-rings in a cubic manner. The most likely division of the unit cell into structural units corresponding to the terrace heights observed by AFM is that the 0.9 ± 0.1 nm terrace corresponds to a sodalite cage and the 0.3 ± 0.1 nm terrace corresponds to

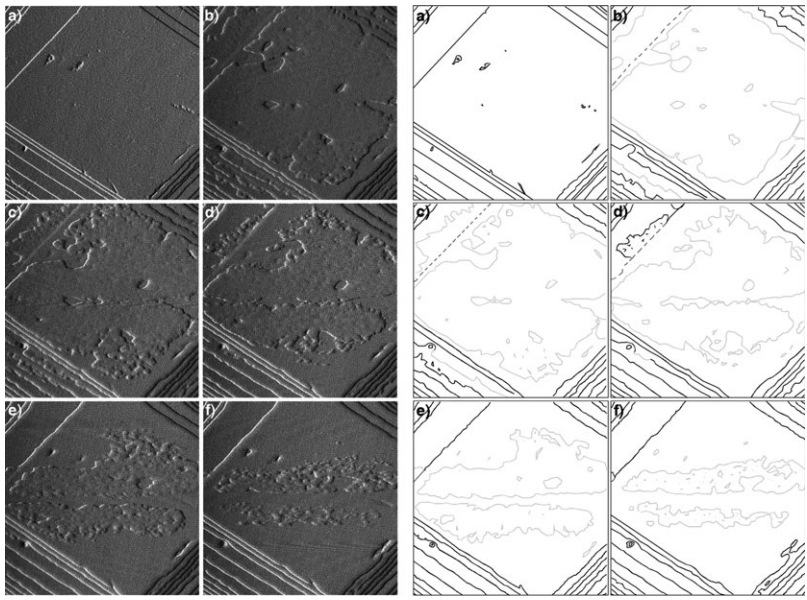

Fig. 2 Left: 4.3 × 4.3 μm^2 deflection AFM images of a zeolite A crystal under NaOH 0.5 M at 0, 31, 33, 36, 38 and 47 min. Right: schematic representation showing the dissolution process observed in the left AFM images. The black lines correspond to step heights of 1.2 nm, grey areas represent layers with step heights *ca.* 0.9 nm and dashed lines correspond to step heights of *ca.* 0.3 nm.

the addition of a single 4-ring. As the sodalite cages are connected to each other parallel to the (110) facet it is not surprising that they dissolve in a correlated fashion, *i.e.* by terrace retreat. One sodalite cage must be dissolved to expose the next sodalite cage. However, the single 4-rings are not connected to each other and consequently they should dissolve in an uncorrelated manner. This will be impossible to distinguish by AFM as the single 4-rings have a lateral dimension of only

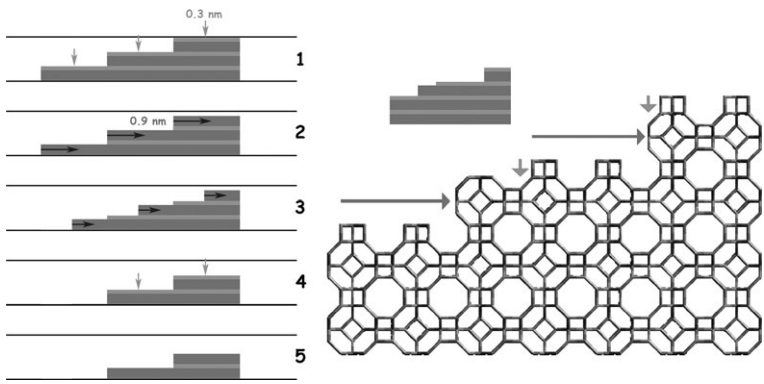

Fig. 3 Schematic illustration of the dissolution process for zeolite A under alkaline conditions. Uncorrelated removal of a single 4-ring capping the double 4-ring shown on the surface of the structure (right, vertical arrow) amounts to 0.32 nm. Correlated removal of a β-cage cage, except the 4-ring base, amounts to 0.92 nm. Layers are successively removed, 4-rings orthogonal to surface and β-cage cages parallel to surface *via* terrace retreat. The process is either 1–2–3–4 repeat or 2–3–4–5 repeat depending on the initial exterior surface of the crystal. Note how the top surfaces of 1 and 4 or 2 and 5 are only displaced orthogonal to the surface by 1.2 nm and therefore indistiguishable by AFM.

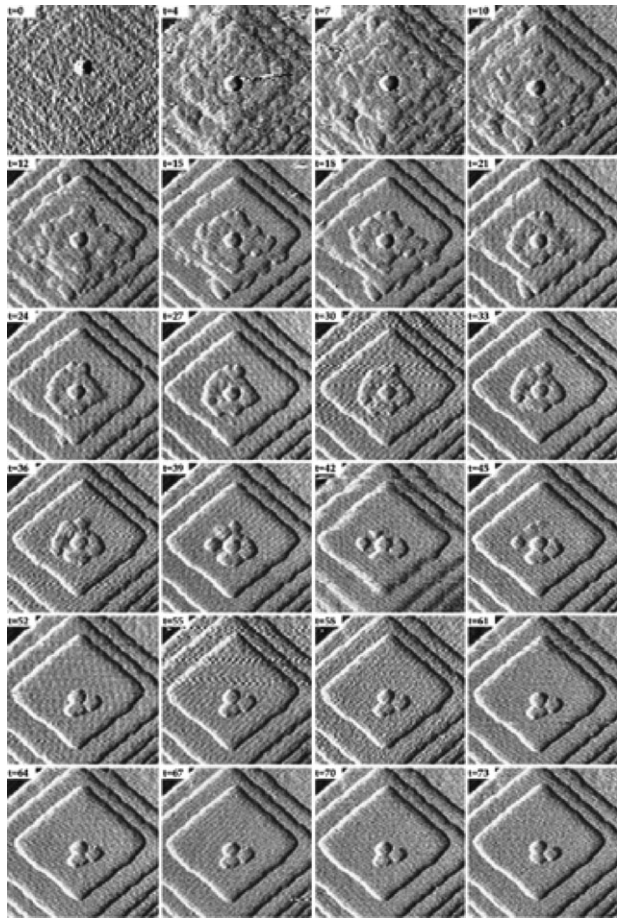

Fig. 4 Series of 1 × 1 μm^2 deflection AFM micrographs of a zeolite A crystal under a static solution of mother liquor diluted to 67%. Images from 0–73 min.

ca. 0.3 nm and the lateral resolution of the AFM is typically *ca.* 3 nm. These two structural terminations for zeolite A are consistent with the theoretical work of Slater *et al.*[15] who calculate that these are the energetically preferred surface structures.

Another feature of this mechanism of dissolution in zeolite A is that periodically the terrace configuration returns to the same lateral topology (compare schematic 1 and 4 or schematic 2 and 5). This is a result of the difference in kinetics of dissolution of the two processes. The dissolution of the single 4-rings is sufficiently slow to arrest the terrace retreat of the sodalite cages essentially at the same position as the preceding terrace edge. This is observed experimentally and explained well by our model of zeolite dissolution.

A similar dissolution process is observed when zeolite A is exposed to an undersaturated mother liquor solution, diluted to 67%, as seen in Fig. 4. Particularly apparent in this series of images is the final break up of the retreating 0.9 ± 0.1 nm high terrace into small, rather uniform squares each with *ca.* 90 × 90 nm lateral dimension. This rather strange phenomenon suggests that at this critical size the free energy of these nano-slabs is a minimum and therefore stabilised. The final dissolution of these units is then rapid but not by terrace retreat. Theoretical modelling of this phenomena would be useful to understand the interplay of both entropic and enthalpic contributions to this stabilisation.

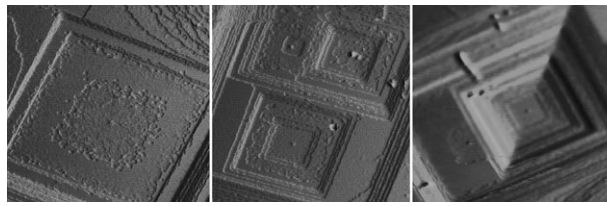

Fig. 5 Deflection AFM images of a zeolite A crystal (a) 4.1 × 4.1 μm^2 under a static solution of mother liquor diluted to 50%, (b) 4.0 × 4.0 μm^2 under a continuous flow solution of mother liquor diluted to 10%, (c) 5.0 × 5.0 μm^2 under a static solution of mother liquor 100%.

Defects and crystal growth in zeolite A

Crystals of zeolite A often have a tendency to exhibit pyramids of terraces all seemingly emanating from the same point on the crystal surface. Dissolution of zeolite A also reveals another interesting feature. Owing to the preferential dissolution of defects in the material it is revealed that there is a defect at the centre of each pyramid, see Fig. 5. The exact nature of this defect is not clear and is observed in the AFM simply as a depression in the surface. Because the AFM tip is unable to penetrate deep into such a small hole it is impossible to ascertain the full depth of the defect, however, intuitively it is expected that it will penetrate at least the depth of the exposed pyramid. Such line defects would be extremely difficult to observe using electron microscopy owing to the rather unstable nature of zeolite A in the electron beam, however, it would be of interest to try to locate these on siliceous forms of zeolite A which should be substantially more beam stable. Electron microscopy might give a better understanding of the fine structural nature at such defects. Our work shows, however, that AFM is a very straightforward technique for locating defects which emanate at the crystal surface and that selective dissolution at the defect sites is a useful strategy to expose otherwise topographically hidden defects.

As well as defect initiated layer growth in zeolite A in some cases we also observe spiral growth from screw dislocations. Similar spiral growth has been reported before for the natural zeolite heulandite.[16] The nature of possible screw dislocations in zeolites has been discussed and modelled by Slater *et al.*[17] Owing to the large unit cell parameter for a zeolite, 2.4 nm for zeolite A, it is necessary for a screw dislocation to spiral around a mesoscopic void or substantially twisted structural conformation. This is rather different to a screw dislocation in a metallic crystal which simply requires a simple displacement of atoms close to the dislocation line. Slater *et al.*[17] showed how it was possible to twist the structure in such a way that essentially no mesoscopic void is created but there is a knock on effect to the structural twisting for several unit cells away from the dislocation line. The AFM shown in Fig. 6 shows that the screw dislocation is often accommodated around a more substantial mesoscopic void *ca.* 60 nm diameter, equivalent to *ca.* 25 unit cells. This should certainly be sufficient for relaxation of the structure. We have also observed spiral growth where any mesoscopic void present is below the lateral resolution of the AFM tip and so we can certainly not rule out the possibility of Slater-type screw dislocations. The predominant growth mechanism in zeolite A is, however, layer-by-layer growth and growth at screw dislocations can be viewed as an important but subsidiary mechanism.

Supersaturation and controlling layer growth

The key to control over defects, intergrowths, crystal habit *etc.* is to be able to control fundamental growth processes independently of each other. This can either be achieved by enhancing or retarding certain growth processes or by facilitating

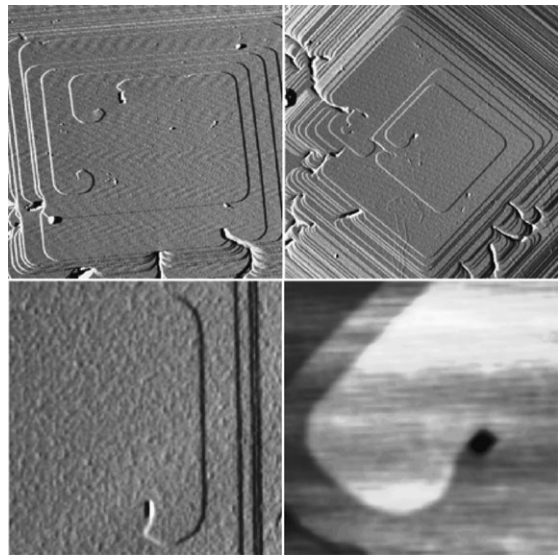

Fig. 6 Spirals observed on the {100} faces of zeolite A: top images AFM deflection images with scan sizes of (left) 4 × 4 μm, (right) 6 × 6 μm, lower images zoomed.

completely new avenues for crystal growth. In this work we demonstrate how supersaturation can be used to effectively control the nucleation of events *versus* the spreading of surface terraces. The principle of this strategy is that different fundamental processes have different activation energies. By changing supersaturation, or temperature, it is possible to change the rates of these processes. However, because the rates vary in a non-linear fashion, and the response to changes in supersaturation is dependent upon activation energy it is possible to alter relative rates for different processes.

A simplistic view of the growth of a zeolite crystal is depicted in Fig. 7a and b. The figure shows how the crystal size and growth rate varies as a function of supersaturation. At the beginning of a crystallisation a silica source is dissolved in a basic medium. During this period the supersaturation level is low and the crystals remain small. However, as the supersaturation level grows so does the crystal growth rate until a steady-state is reached at constant supersaturation and constant growth rate. During this period the crystal length increases linearly with time. Finally the silica nutrient is exhausted and the saturation level drops and the crystals eventually cease to grow. Crystals removed from a growth medium at the end of a synthesis would exhibit surface features consistent with growth under low supersaturation conditions. In order to control the supersaturation conditions we have grown crystals under conditions of constant supersaturation using a continuous flow autoclave. Nutrient is continually fed in to the vessel at the same rate as the nutrient is being depleted by crystal growth.

The model system we have chosen for study is the siliceous microporous material, silicalite. Silicalite has a two dimensional medium pore system and the orthorhombic crystal symmetry is manifested in crystals with two flat facets and a circular facet, see Fig. 7c. This morphology is consistent with crystals which have low levels of defects and faulting. The crystal growth was conducted in a manner whereby the supersaturation was maintained at a high level, area shaded in Fig. 7a, and then the level allowed to drop, area shaded in Fig. 7b. This was repeated twice such that the supersaturation level was allowed to drop after 9.6 and 16.4 h. Fig. 7c shows scanning electron micrographs, reproduced to scale, of the crystals removed after various periods of time. The crystals grow in a highly linear fashion while the

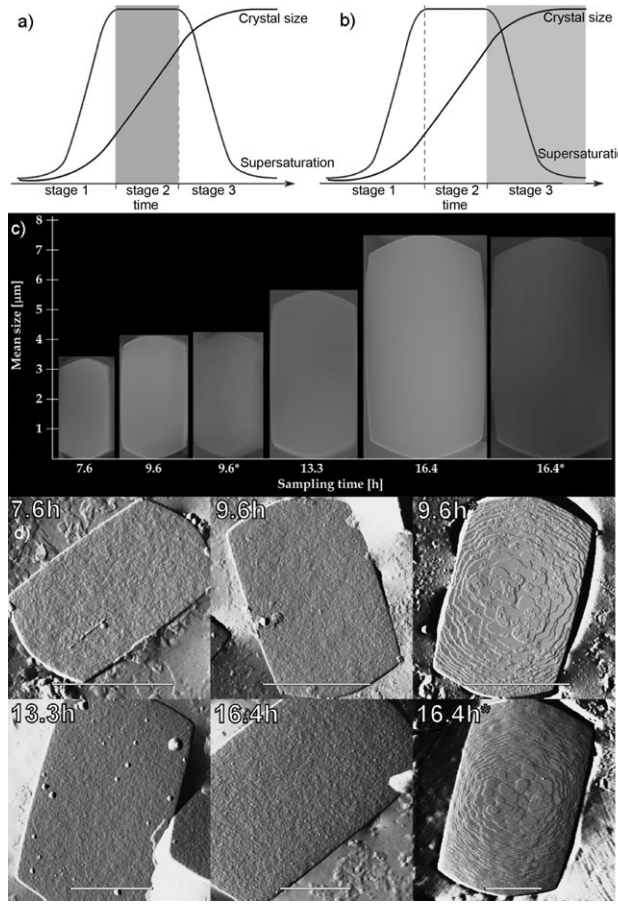

Fig. 7 Parts (a) and (b) show a schematic representation of the supersaturation and crystal length changes during crystal growth; (c) series of scanning electron micrographs of silicalite crystal grown under continuous nutrient feed conditions, times marked with an asterisk show when the nutrient feed was switched off; (d) series of AFM images of the (010) facet of silicalite.

supersaturation is high and the crystals almost cease growing when the supersaturation level is allowed to drop. Fig. 7d shows a series of AFM images of the (010) surface of this set of crystals. What is most noticeable is the substantial difference in the surface topology when the supersaturation drops, times 9.6* and 16.4* h. In these images 1 nm high terraces are clearly distinguished and the concentration of nucleation events is fairly low. In contrast, in the AFM images recorded when the supersaturation level is high, the crystal surface has a high density of surface nucleation events without clearly established terraces. These images indicate that when the supersaturation level is dropped the first process to be limited is surface nucleation, the event which will have the highest activation energy. However, surface spreading continues and the surface roughness grows out. This effect can be seen more clearly in the following section where we have simulated the surface topology *via* crystal growth models.

With silicalite growth conditions have been established whereby it is possible to selectively turn off the process with the highest activation energy while maintaining growth *via* less energy expensive processes. If this is a general phenomena then it offers an excellent prospect for controlling intergrowth and defect populations which

are often the result of the competitive layer nucleation and layer spreading processes. Such is the case for the important intergrowth system hexagonal and cubic zeolite Y (structure codes EMT/FAU).[18] It may also be illustrated with reference to the microporous titanosilicate system ETS-10 which was referred to in the Introduction.[9] ETS-10 is a system which is built from layers and contains both well defined defects as well as an intergrowth structure resulting from a random stacking of these layers. The layers are themselves composed of rods of titanate chains surrounded by a silica network, Fig. 8. However, if we initially consider the layer growth as depicted on the high-resolution electron micrograph in Fig. 8 then the different colour circles show the pore structure in the different layers. The layer depicted at the bottom of the micrograph in white has three layers above. These are a result of multiple nucleation such that the layer does not spread fast enough to ensure complete coverage. If the multiple nuclei are displaced relative to each other then at the boundary where the nuclei meet a defect is created which is manifested as a double pore. This mechanism then repeats. In order to decrease the level of defects it would be necessary to decrease the nucleation rate relative to the spreading rate, in a similar manner to that already achieved in the silicalite system. If it were possible to achieve the opposite such that the rate of nucleation was increased relative to the spreading rate then the concentration of double-pore defects could in principle be increased.

Controlling the intergrowth structure requires controlling the stacking sequence which will require making one polymorph more energetically favoured. This will probably require a template either to force a particular polymorph or poison a particular polymorph.

The situation in ETS-10 is further complicated because the crystal actually grows from a succession of rods rather than layers and this results in another type of defect

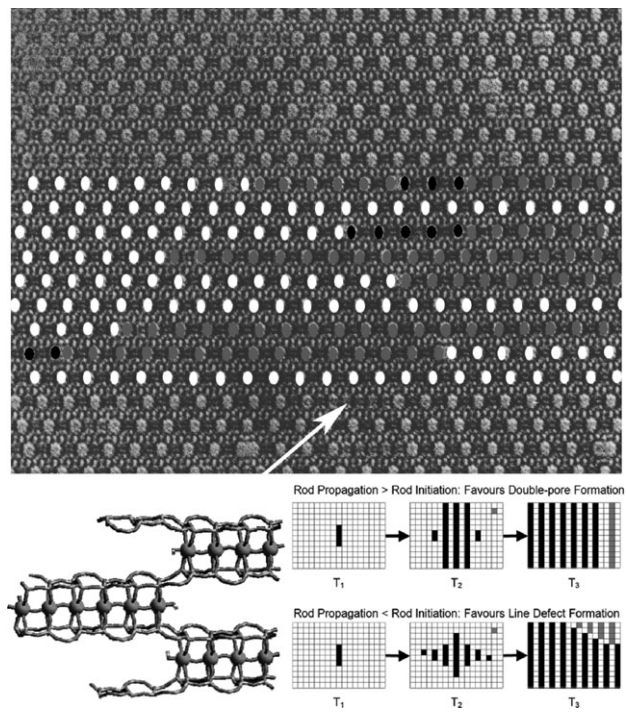

Fig. 8 Top image shows a high-resolution electron micrograph with pore arrangement white, grey or black to illustrate layer nucleation and spreading to incorporate defects; below show rod structure in ETS-10 and how the rods nucleate defects.

illustrated by the white arrow in Fig. 8. Here the pores appear to be blocked and is a result of interruption in the rod structure as shown in Fig. 8. The density of such defects is very high, indeed too high to be caused as a result of a random stacking of rods resulting from the relative nucleation and spreading rates of the rods. Consequently it is necessary to invoke a further possible scenario that the rod ends (the black rods in Fig. 8) act as nucleation points for the displaced rods (grey rods in Fig. 8). This last point is made both to illustrate the complexity of crystal growth in nanoporous materials, but also to illustrate that we are able to disentangle much of this complexity by combining, in particular, modern microscopic techniques.

Simulation of crystal habit and surface topology in nanoporous materials

Ultimately, the atomic force micrographs contain important information not only about growth mechanism but also about growth rates and activation energies for growth. However, extracting such information is far from straightforward. Our approach to at least partially tackle this problem is to try to simulate the surface topology *via* computer models. Similar approaches have been adopted in the past for other systems such as water[19] and urea.[20] An added complication with nanoporous materials is that it is still not clear from which solution species the crystals grow. Basic silicate solutions exhibit a plethora of oligomeric silicate species, the concentration and nature of which vary according to temperature, pH and the presence of organic structure directing agents.[13] Many of these species will be spectators and the true nature of the active species is still unclear. Consequently, we have chosen not to consider the primary growth unit as the unit for our modelling. Instead we have chosen closed cage structures which we know from the surface topology (AFM and HREM) are preferred surface structures. As the structures are, at least, metastable these structures can be considered rate determining and consequently it is not necessary to consider smaller, more fundamental, growth units. This simplifies the modelling considerably. However, even with this simplification in parameterisation the growth model will still have far more independent variables than parameters to which the model can be tested. In order to increase the level of input to the model from experiment we perform a three-dimensional simulation whereby crystal habit is simulated concurrently with surface topology. The input to the model are the probabilities for growth at structurally different types of sites. These probabilities equate with the fundamental rates in a model such as the one used by Gale *et al.* in the simulation of the crystal growth of urea.[20]

A hard-wired model has been developed for cubic zeolite systems such as zeolite A or sodalite, however, we are in the process of developing a general program, based on the same philosophy which can be applied to any crystal symmetry and connectivity network. Previous two-dimensional models have successfully predicted the topology and density of surface terraces and from this information derived the relative rates of surface nucleation *versus* terrace spreading.[8] Those models were based upon a first nearest neighbour difference in attachment energies. The three-dimensional model, however, invokes a second-nearest neighbour difference in attachment energies which is necessary in order to simulate facets with indices higher than (100). A few examples of the type of growth sites considered in our modelling program are illustrated in Fig. 9. For example, growth site 2_8 has two nearest neighbours and 8 second nearest neighbours. Such a site is not necessarily unique and there will be topologically distinct sites with the same co-ordination, however, for this model they are considered to be degenerate. Fig. 9 shows some of the sites considered on both the (100) and (110) facets. The model will effectively simulate facets up to the (111) index. There are some sixty site types in this description which illustrates the problem of undetermination. As a consequence we apply some strict interrelationships between the probabilities for growth

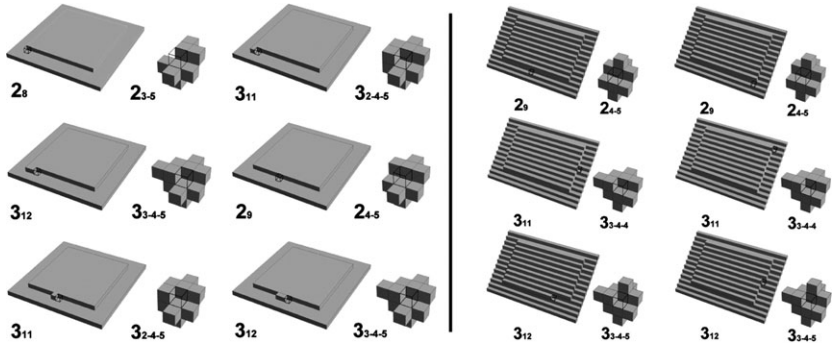

Fig. 9 A sample of the site types used in the modelling of zeolite A growth. Main number is the first-nearest-neighbour connectivity and the subscript the second-nearest-neighbour connectivity.

at the various sites. First the primary consideration for growth probability is the first nearest neighbour coordination. The higher the coordination the more probable the growth. Second sites with a first nearest neighbour coordination greater than three are assigned a probability which is so high, relatively, that they are now rate determining and can effectively be eliminated from consideration. Also, a number of sites with low second nearest neighbour coordination are only important in the early stages of crystal growth and are non-effectual in the later important stages of crystal growth. Finally, the probabilities for growth are arranged in sequence according to second nearest neighbour coordination. With all these restrictions the problem becomes determinable.

Fig. 10 shows the result of one simulation of a 0.26 μm crystal. The series incorporates a change in probabilities to simulate a dramatic decrease in the rate of surface nucleation relative to surface spreading. Although the simulation is essentially for zeolite A this is the situation which was encountered in the previous section for silicalite. Two consequences are immediately apparent. First the facetting of the crystal becomes pronounced. Second the multiple nucleation on the crystal surface ceases and the speeding of these nuclei result in a surface with a low population of well-defined square terraces. This is very similar to the result observed for silicalite and shown in Fig. 7. Terracing is also observed on both the (100) and (110) crystal surfaces, the latter similar to that observed in the high-resolution scanning electron micrographs reported by Sacco *et al.*[21] A much more detailed description of these results and calculations of activation energies for fundamental processes in zeolite A will be reported elsewhere.[22]

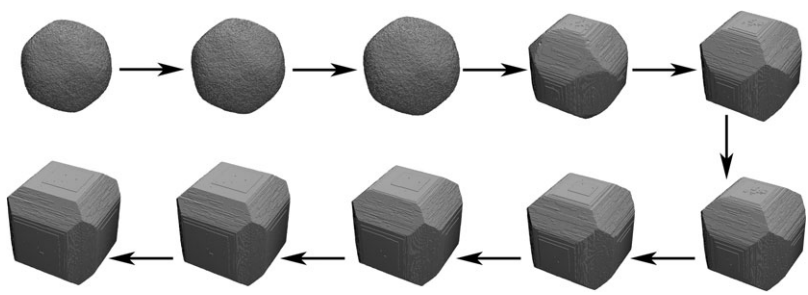

Fig. 10 10 000 000 iterations to grow a 0.26 μm zeolite crystal. The probabilities are switched to show the effect of suppression of surface nucleation.

Conclusions

In conclusion we have shown that atomic force microscopy, recorded both *ex situ* and *in situ* is a valuable tool to understand fundamental growth processes in nanoporous materials. When coupled with computer simulation it is possible to determine the underlying mechanisms and ultimately activation energies for these processes. By altering crystal growth conditions it is possible to switch processes on and off relative to one another and this is demonstrated for the nanoporous silicate silicalite.

References

1 C. S. Cundy and P. A. Cox, *Chem. Rev.*, 2003, **103**, 663.
2 C. S. Cundy and P. A. Cox, *Microporous Mesoporous Mater.*, 2005, **82**, 1.
3 M. E. Davis, *Nature*, 2002, **417**, 813.
4 O. Larlus and V. P. Valtchev, *Chem. Mater.*, 2004, **16**, 3381.
5 D. E. Akporiaye, I. M. Dahl, A. Karlsson and R. Wendelbo, *Angew. Chem., Int. Ed.*, 1998, **37**, 609.
6 W. M. Meier, in *Atlas of Zeolite Framework Types*, ed. Ch. Baerlocher, W. M. Meier and D. H. Olson, Elsevier, Amsterdam, 5th edn, 2001.
7 G. Binnig, C. F. Quate and C. Gerber, *Phys. Rev. Lett.*, 1986, **56**, 930.
8 J. R. Agger, N. Pervaiz, A. K. Cheetham and M. W. Anderson, *J. Am. Chem. Soc.*, 1998, **120**, 10754.
9 M. W. Anderson, O. Terasaki, T. Ohsuna, P. J. O'Malley, A. Philippou, S. P. MacKay, A. Ferreira, J. Rocha and S. Lidin, *Philos. Mag. B*, 1995, **71**, 813.
10 Collaboration funded by EPSRC.
11 P. Bussian, F. Sobott, B. Brutschy, W. Schrader and F. Schüth, *Angew. Chem., Int. Ed.*, 2000, **39**, 3901.
12 C. S. Cundy, M. S. Henty and R. J. Plaisted, *Zeolites*, 1995, **15**, 353.
13 A. V. McCormick, A. T. Bell and C. J. Radke, *Zeolites*, 1987, **7**, 183.
14 C. Serre, C. Lorentz, F. Taulelle and G. Ferey, *Zeolites*, 2003, **15**, 2328.
15 B. Slater, J. O. Titiloye, F. M. Higgins and S. C. Parker, *Curr. Opin. Solid State Mater. Sci.*, 2001, **5**, 417.
16 L. Scandella, N. Kruse and R. Prins, *Surf. Sci.*, 1993, **281**, L331.
17 A. M. Walker, B. Slater, J. D. Gale and K. Wright, *Nat. Mater.*, 2004, **3**, 715.
18 J. M. Newsam, M. M. J. Treacy, D. E. W. Vaughan, K. G. Strohmaier and W. J. Mortier, *J. Chem. Soc., Chem. Commun.*, 1989, 493.
19 B. Wathen, M. Kuiper, V. Walker and Z. Jia, *J. Am. Chem. Soc.*, 2003, **125**, 729.
20 S. Piana, M. Reyhani and J. D. Gale, *Nature*, 2005, **438**, 70.
21 S. Bazzana, S. Dumrul, J. Warzywoda, L. Hsiao, L. Klass, M. Knapp, J. A. Rains, E. M. Stein, M. J. Sullivan, C. M. West, J. Y. Woo and A. Sacco, Jr, *Stud. Surf. Sci. Catal.*, 2002, **142A**, 117.
22 C. Chong, PhD Thesis, University of Manchester, 2007C. B. Chong, J. R. Agger and M. W. Anderson, in preparation.

